

Core-modified rubyrins with phenanthrene-fused pyrrole rings: Highly selective and tunable response to Hg^{2+} ions

Xuemei Yuan^a, Minzhi Li^b, Ting Meng^a, John Mack^{c,**}, Rodah Soy^c, Tebello Nyokong^c, Weihua Zhu^b, Haijun Xu^{a,***}, Xu Liang^{b,d,*}

^a College of Chemical Engineering, Jiangsu Key Lab of Biomass-based Green Fuels and Chemicals, Nanjing Forestry University, Nanjing 210037, PR China

^b School of Chemistry and Chemical Engineering, Jiangsu University, Zhenjiang 212013, PR China

^c Centre for Nanotechnology Innovation, Department of Chemistry, Rhodes University, Grahamstown 6140, South Africa

^d State Key Laboratory of Coordination Chemistry, Nanjing University, Nanjing 210000, PR China

ARTICLE INFO

Keywords:

Rubyrin
Electronic structure
Spectroscopy
 Hg^{2+} ion sensors

ABSTRACT

Three fused-ring-expanded rubyrins with modified macrocyclic core have been synthesized and characterized. A series of spectroscopic, electrochemical measurements and a set of theoretical calculations demonstrate that the core-modification of the inner core of rubyrins has a large influence on the electronic structure. Colorimetric changes are observed that demonstrate that these core-modified rubyrins could be used as selective Hg^{2+} ion sensors. These properties can be fine-tuned by introducing lipophilic substituents on the *meso*-aryl rings.

1. Introduction

In the past 20 years, a wide range of novel expanded porphyrin structures have been successfully synthesized and characterized by using a number of different structural modification strategies such as, macrocycle ring-expansion, the introduction of heterocycles other than pyrrole (core modification), *meso*-substitution, and heterocycle inversion (i.e. “confused” porphyrins) [1–3]. Core-modified expanded porphyrins in which heteroatoms replace the pyrrole nitrogens have seldom been studied despite being particularly attractive due to the large influence that this structural modification strategy has on the aromatic properties of the electronic structure [4–6]. The degree of aromaticity of core-modified porphyrinoids can be quantified by experimental characterization and theoretical calculation by studying the molecular and electronic structures, and the external magnetic field induced diamagnetic ring current. For example, expanded porphyrins could be explored by various spectroscopic and electrochemical techniques [7–9]. On the other hand, the electronic structure of expanded porphyrinoids can also be easily predicted by theoretical calculations such as the use of molecular orbital (MO) theory, nucleus-independent chemical shift (NICS) and anisotropy of the current-induced density (ACID), and these approaches can be used to determine the extent to which a novel macrocycle is aromatic [10,11].

Typically, porphyrins can be regarded as aromatic molecules that

follow Huckel's ($4N + 2$) rule containing 18π -electrons delocalized on the inner ligand perimeter [10]. Thus, the connection between the electronic structures of core-modified expanded porphyrinoids and their properties can be rationalized by using conceptual frameworks such as Gouterman's 4-orbital [12] and Michl's perimeter model [13–17] that consider how structural modifications change the relative energies of the MOs that are derived from the HOMO and LUMO of a D_{16h} symmetry $\text{C}_{16}\text{H}_{16}^{2-}$ parent hydrocarbon cyclic perimeter. As a relatively new class of functional molecules, ring-expanded porphyrinoids have attracted considerable attention recently as selective anion receptors, ligands for transition and lanthanoid ions, use as photosensitizers in photodynamic therapy and magnetic resonance imaging contrast agents [18]. Expanded macrocycles of this type have also proven useful in the study of aromatic effects in large heteroannulenes, while, more recently, their large two-photon absorption cross sections, have made these compounds attractive for use in the study of three-dimensional micro-fabrication, optical data storage, and optical limiting effects [19–22].

Herein, we report an in-depth analysis of the optical properties of fused-ring-expanded rubyrins ([26]hexaphyrins (1.1.0.1.1.0)) that are core-modified with group 16 heteroatoms. The Hg^{2+} ion is known to be a ubiquitous heavy-metal pollutant and one of the most toxic metal ions in the environment, which ranks sixth among the most toxic chemicals in the list of hazardous compounds [23]. Hg^{2+} can cause many kinds of

* Corresponding author. School of Chemistry and Chemical Engineering, Jiangsu University, Zhenjiang 212013, PR China. Tel.: +86 511 8879 1928.

** Corresponding author.

*** Corresponding author.

E-mail addresses: j.mack@ru.ac.za (J. Mack), xuhaijun@njfu.edu.cn (H. Xu), liangxu@ujs.edu.cn (X. Liang).

diseases in the brain, heart, kidneys, lungs, central nervous system, and immune system in humans even at ppm levels of mercury accumulation [24]. The development of highly selective and sensitive optical probes for the detection of Hg^{2+} is of great significance for both the environment and human health. In recent years, the design and construction of optical sensors for the recognition of Hg^{2+} has attracted considerable attention [25]. In this manuscript, the effect of fused-ring-expansion, ring-expansion of the macrocycle and the electron-donating properties of *meso*-aryl substituents on their electronic structures through various spectroscopic and electrochemical measurements, and theoretical applications.

2. Results and discussion

2.1. Materials and methods

Unless otherwise noted, all chemicals and solvents were of commercial reagent grade and used without further purification. Dry dichloromethane was freshly distilled over CaH_2 under nitrogen. Dry *n*-hexane and THF were distilled from sodium/benzophenone under an inert atmosphere. Elemental analyses for C, H and N, were performed on a Perkin-Elmer 240 C elemental analyzer. ^1H NMR spectra were recorded on a Bruker DRX300 and DRX600 spectrometer at ambient temperatures. The chemical shifts are expressed relative to TMS as the internal standard. MALDI-TOF-MS experiments were performed using an Applied Biosystems 4800 proteomics analyzer equipped with an Nd:YAG laser operating at the third harmonic wavelength of 355 nm, a repetition rate of 200 Hz, and an acceleration voltage of 20 kV. ESI-HRMS measurements were carried out using a Thermo Fisher Scientific LTQ Orbitrap XL, USA. 2,2'-bithiophene (1a) [26], *p*-hexadecyloxybenzaldehyde [27] and phenanthropyrrole [28] were prepared according to the literature methods. Cyclic voltammetry was carried out on a Chi-730D electrochemistry station with a three-electrode cell. A glassy carbon disk, a platinum wire and an Ag/AgCl electrode were used as the working, counter and reference electrodes, respectively. The UV and visible regions of the electronic absorption spectra were recorded with an HP 8453A diode array spectrophotometer.

2.2. General synthetic procedure

2.2.1. Preparation of diols

n-Hexane (90 mL) was added to a 250 mL three-necked round-bottomed flask flushed with argon for 10 min. TMEDA (1.8 mL, 11.4 mmol) and *n*-BuLi (7.2 mL of ca. 1.6 M solution in hexane, 11.4 mmol) were then added, and the solution was stirred under argon for 10 min. 2,2'-bithiophene (3.82 mmol) was added, and the solution was gently refluxed for 1 h. The reaction mixture was then allowed to attain 25 °C. The reaction mixture was cooled to 0 °C in an ice bath, and then a solution of aromatic aldehyde (9.53 mmol) in THF (25 mL) was added dropwise. After the addition was over, the reaction mixture was stirred at 0 °C for 15 min and then brought to room temperature. The reaction was quenched by adding an ice-cold saturated NH_4Cl solution (40 mL), and it was then extracted with CHCl_3 (50 mL \times 3). The organic layers were combined and washed with water and brine solution and dried over anhydrous Na_2SO_4 . The solvent was removed in a rotary evaporator under reduced pressure to obtain the crude compound, which was recrystallized from CHCl_3 /*n*-hexane to afford the diol as a pale white solid (Scheme 1).

2.2.2. Preparation of rubein 3a-e

The appropriate diol (0.5 mmol) was added to a stirred solution of phenanthropyrrole (107 mg, 0.5 mmol) in freshly dry deoxygenated dichloromethane (80 mL), and the resulting solution was purged with argon for 10 min. After addition of boron trifluoride etherate (80 μL , 0.64 mmol) the reaction mixture was stirred for 1 h at -50°C in the dark, and then warmed to room temperature for 48 h. The resulting

solution was opened to air and 2,3-dichloro-5,6-dicyano-1,4-benzoquinone (DDQ, 227 mg, 1 mmol) was added, and the mixture was stirred for a further 1 h. The solvents were removed under reduced pressure by rotary evaporation. The crude product was purified by silica-gel flash column chromatography and recrystallization from chloroform/methanol afforded the rubein as deep blue solid (Scheme 1). ^1H NMR spectroscopy and MS (ESI-HR, MALDI-TOF) are provided in the Supporting Information (see ESI).

2.3. Structural characterization

5,5'-Bis(phenylhydroxymethyl)-2,2'-bithiophene (2a): 0.95 g, 66%; ^1H NMR (300 MHz, DMSO-d_6): δ 7.41 (d, $J = 7.5$ Hz, 4 H, phenyl-*H*), 7.33 (t, $J = 7.5$ Hz, 4 H, phenyl-*H*), 7.24 (dd, $J = 6.9, 7.2$ Hz, 2 H, phenyl-*H*), 6.98 (d, $J = 3.6, 2$ H, thiophene-*H*), 6.76 (d, $J = 3.6, 2$ H, thiophene-*H*), 5.86 (s, 2 H, -CH-). ^{13}C NMR (75 MHz, DMSO-d_6): δ 149.9, 114.9, 136.1, 128.6, 127.7, 126.5, 125.1, 123.2, 70.8.

5,5'-Bis(4-*tert*-butyl-phenylhydroxymethyl)-2,2'-bithiophene (2b): 1.03 g, 55%; ^1H NMR (300 MHz, DMSO-d_6): δ 7.30–7.36 (dd, $J = 9.0, 10.2$ Hz, 8 H, phenyl-*H*), 6.98 (d, $J = 3.6$ Hz, 2 H, thiophene-*H*), 6.76 (d, $J = 3.6$ Hz, 2 H, thiophene-*H*), 5.83 (s, 2 H, -CH-), 1.25 (s, 18 H, -*t*-Bu-*H*). ^{13}C NMR (75 MHz, DMSO-d_6): δ 150.0, 142.1, 136.0, 126.2, 125.4, 124.9, 123.2, 70.8, 57.5, 31.6.

5,5'-Bis(4-hexadecyloxy-phenylhydroxymethyl)-2,2'-bithiophene (2c): 1.25 g, 38%; ^1H NMR (600 MHz, DMSO-d_6): δ 7.29 (d, $J = 12.6$ Hz, 4 H, phenyl-*H*), 6.96 (d, $J = 4.8$ Hz, 2 H, thiophene-*H*), 6.86 (d, $J = 12.6$ Hz, 4 H, phenyl-*H*), 6.73 (d, $J = 4.8$ Hz, 2 H, thiophene-*H*), 6.16 (br, 2 H, -OH), 5.81 (s, 2 H, -CH-), 3.92 (t, $J = 9.6$ Hz, 4 H, -OCH₂-), 1.64–1.61 (m, 4 H, -OCH₂-CH₂-CH₂-), 1.34–1.42 (m, 4 H, -CH₂-), 1.23 (s, 44 H, -CH₂-), 1.14 (s, 4 H, -CH₂-), 0.85 (t, $J = 9.0, 10.2$ Hz, 6 H, -CH₃).

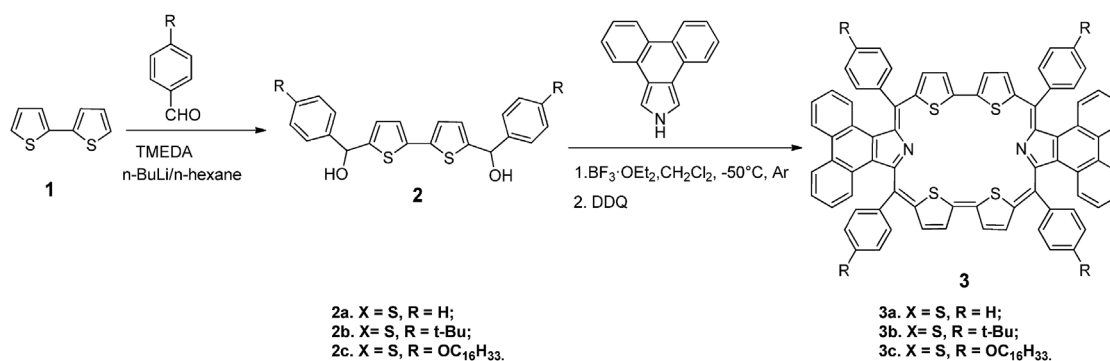
Tetrathiarubein (3a): 89 mg, 32%; ^1H NMR (600 MHz, CDCl_3): δ 9.48–9.49 (br, 4 H, thiophene-*H*), 9.36–9.37 (br, 4 H, thiophene-*H*), 8.68–8.69 (m, 8 H, meso-phenyl-*H*), 8.57 (d, $J = 7.8$ Hz, 4 H, meso-phenyl-*H*), 8.23 (d, $J = 8.4$ Hz, 4 H, meso-phenyl-*H*), 7.79 (dd, $J = 7.2, 6.6$ Hz, 8 H, fused ring-*H*), 7.65 (dd, $J = 6.6, 7.2$ Hz, 4 H, meso-phenyl-*H*), 7.39 (dd, $J = 6.6, 7.2$ Hz, 4 H, fused ring-*H*), 7.12 (dd, $J = 7.8, 7.2$ Hz, 4 H, fused ring-*H*) ppm. Anal. Calcd. (%) for $\text{C}_{76}\text{H}_{44}\text{N}_2\text{S}_4$: C, 81.98; H, 3.98; N, 2.52; found: C, 82.02; H, 3.94; N, 2.55. ESI-HRMS: $[\text{M} + \text{H}]^+ = 1113.2537$ (Calcd. $[\text{M} + \text{H}]^+ = 1113.2460$). ϵ ($\text{L}\cdot\text{mol}^{-1}\cdot\text{cm}^{-1}$): 595 (71000), 716 (8600), 779 (9100).

Tetrathiarubein (3b): 98 mg, 29%; ^1H NMR (600 MHz, CDCl_3): δ 8.87–8.88 (br, 8 H, thiophene-*H*), 8.57 (d, $J = 7.8$ Hz, 4 H, meso-phenyl-*H*), 8.42 (s, 8 H, meso-phenyl-*H*), 7.92 (d, $J = 7.8$ Hz, 4 H, meso-phenyl-*H*), 7.71 (d, $J = 7.8$ Hz, 8 H, fused ring-*H*), 7.37 (dd, $J = 6.6, 6.6$ Hz, 4 H, fused ring-*H*), 7.06 (dd, $J = 6.6, 7.2$ Hz, 4 H, fused ring-*H*), 1.51 (s, 36 H, *t*-Bu-*H*) ppm. Anal. Calcd. (%) for $\text{C}_{92}\text{H}_{76}\text{N}_2\text{S}_4$: C, 82.59; H, 5.73; N, 2.09; found: C, 82.55; H, 5.77; N, 2.14. ESI-HRMS: $[\text{M} + \text{H}]^+ = 1337.5096$ (Calcd. $[\text{M} + \text{H}]^+ = 1337.4964$). ϵ ($\text{L}\cdot\text{mol}^{-1}\cdot\text{cm}^{-1}$): 595 (87000), 719 (9500), 788 (14500).

Tetrathiarubein (3c): 217 mg, 42%; ^1H NMR (600 MHz, CDCl_3): δ 9.08–9.09 (br, 4 H, thiophene-*H*), 8.86–8.89 (br, 4 H, thiophene-*H*), 8.50 (d, $J = 6$ Hz, 12 H, meso-phenyl-*H*), 8.00–8.01 (d, $J = 2.4$ Hz, 4 H, meso-phenyl-*H*), 7.32 (s, 4 H, fused ring-*H*), 7.24–7.26 (m, 8 H, fused ring-*H*), 7.06 (t, $J = 6$ Hz, 4 H, fused ring-*H*), 4.13 (s, 8 H, -OCH₂-), 1.89 (ddd, $J = 7.2, 7.2, 6.6$ Hz, 8 H, -OCH₂-CH₂-), 1.55–1.57 (m, 16 H, -CH₂-), 1.43–1.44 (m, 8 H, -CH₂-), 1.26–1.29 (m, 80 H, -(CH₂)-), 0.88–0.90 (t, $J = 7.2$ Hz, 12 H, -CH₃) ppm. Anal. Calcd (%) for $\text{C}_{140}\text{H}_{172}\text{N}_2\text{O}_4\text{S}_4$: C, 81.03; H, 8.35; N, 1.35; found: C, 81.07; H, 8.41; N, 1.40. MALDI-TOF-MS: $[\text{M} + \text{H}]^+ = 2074.752$ (Calcd. $[\text{M} + \text{H}]^+ = 2074.227$). ϵ ($\text{L}\cdot\text{mol}^{-1}\cdot\text{cm}^{-1}$): 595 (97000), 716 (10500), 779 (21000).

2.4. Theoretical calculations

B3LYP geometry optimizations were carried out for 3a-c and a series of seven model complexes at the B3LYP/6-31G(d) level of theory by using



Scheme 1. Synthetic procedures for core modified rubyrin 3.

the Gaussian 09 software package. The TD-DFT calculations were carried out in a similar manner by using the CAM-B3LYP functional, which contains a long-range correction. The model complexes include tetraphenylporphyrin (PN₄), tetraphenyldiphenanthroporphyrin (N₄), tetraphenyldithiaporphyrin (PN₂S₂), tetraphenyldiphenanthrodithiaporphyrin (N₂S₂), tetraphenylrubyrin (PN₆), tetraphenyldiphenanthrorubyrin (N₆), tetraphenyltetrathiarubyrin (PS₄N₂) and tetraphenyldiphenanthrotetrathiarubyrin (S₄N₂). To simplify the calculations the structures of 3b and 3c are modified to include methyl (3b-CH₃) and methoxy (3b-OCH₃) groups respectively at the *para*-positions of the *meso*-aryl rings.

3. Results and discussion

3.1. Structural characterization

A series of fused-ring-expanded rubyrins 3a-c that are core-modified with sulfur atoms were synthesized from a reaction of diols and phenanthropyrroles in freshly dried and deoxygenated dichloromethane and were purified by silica gel column chromatography and recrystallization. ESI-HRMS revealed an intense parent peak for 3a at $[M + H]^+ = 1113.2537$ (Calcd. $[M + H]^+ = 1113.2460$) (Fig. S1, see ESI), providing direct evidence that the target compound was successfully prepared. In addition, similar parent peaks of HR-MS were also observed for 3b and 3c (Figs. S2–S3, see ESI). The proton signals for the *meso*-substituents, pyrrole and thiophene rings in the ¹H NMR spectra of 3a-c lie beyond 7.40 ppm (Figs. S4–S6, see ESI). The purity of synthetic compounds was further confirmed by elemental analysis, and the results are fully consistent with the theoretical results.

3.2. Theoretical calculations and optical spectroscopy

Firstly, it is noteworthy that the nodal patterns of the four frontier π -MOs of 3a (Fig. 1) are consistent with what would be anticipated for MOs derived from the HOMO and LUMO of a parent C₂₂H₂₂⁴⁻ aromatic hydrocarbon perimeter with D_{22h} symmetry corresponding to the inner perimeter of the π -system [13–17]. Six angular nodal planes are observed for the HOMO level, and seven for the LUMO level (Fig. 1) as part of an overall M_L = 0, ± 1 , ± 2 , ± 3 , ± 4 , ± 5 , ± 6 , ± 7 , ± 8 , ± 9 , ± 10 , ± 11 , ± 12 , 13 sequence in terms of ascending energy. This is comparable to the M_L = 0, ± 1 , ± 2 , ± 3 , ± 4 , ± 5 , ± 6 , ± 7 , 8 sequence for the C₁₆H₁₆²⁻ parent perimeter of tetraphenylporphyrin that results in frontier π -MOs with four and five angular nodal planes (Figs. 1 and 2). To aid the comparison of compounds with differing symmetries, Michl [13–17] referred to π -MOs derived from the HOMO and LUMO, respectively, that have angular nodal planes that lie on the *y*-axis as the **a** and **-a** MOs, while the MOs that have significant MO coefficients on the *y*-axis are referred to as the **s** and **-s** MOs, respectively. In the context of the parent porphyrin and rubyrin compounds, there are only relatively minor energy splittings of the **a** and **s**, and **-a** and **-s** MOs (the Δ HOMO and Δ LUMO values to use Michl's terminology) relatively weak L (or Q) bands associated with the forbidden Δ M_L = ± 9 or ± 13

transitions between the HOMO and LUMO levels of the π -system and the intense B (or Soret) bands that arise from the allowed Δ M_L = ± 1 transitions are expected to dominate their UV-visible absorption spectra (Fig. 3) [10]. Ring-expansion of the macrocycle results in a narrowing of the HOMO–LUMO gap and a red-shift of the L and B bands (Figs. 2 and 3) [10], and the introduction of fused phenanthro rings to the tetraphenylporphyrin and rubyrin ligands has a similar effect mainly due to a stabilization of the *s* MO due to strong bonding interactions at the points of attachment [5]. In general, the B band of the parent rubyrin compound lies at ca. 550 nm and the L band lies beyond 800 nm. In Fig. 4, rubyrin 3a has an intense B band at 595 nm, while the L bands of 3a lie at 779 and beyond 1100 nm. The introduction of the group 16 heteroatom has a large influence on the electronic structure of rubyrin analogues in a similar manner to what has been observed previously with tetraphenanthroporphyrins [5]. When *tert*-butyl units were introduced at the *meso*-positions of the rubyrin 3b, only minor changes are observed in the B band region, but the L bands are slightly shifted to longer wavelength. The further red-shifts of the B and L absorption bands of rubyrins 3c are consistent with the anticipated trends (Fig. 4), since there is a relative destabilization of the HOMO when electron donating –OR substituents are introduced at the *para*-positions of the *meso*-aryl rings due to the large MO coefficients on the *meso*-carbons (Figs. 1 and 2).

3.3. Electrochemistry

To gain further insight into the electronic structures of 3a-c, cyclic and differential pulse voltammetry (CV and DPV) measurements were carried out in *o*-dichlorobenzene (*o*-DCB) containing 0.1 M tetra-*n*-butylammonium perchlorate ([NBu]ClO₄; TBAP) as a supporting electrolyte, so that redox potential ($E_{1/2}$) values could be derived (Fig. 5). The use of polar solvents including DMF, DMSO and PhCN was found to be problematic due to the poor solubility of the compounds in these solvents. Two reversible reduction curves are observed for 3a in *o*-DCB at –0.63 and –1.70 V, while reversible oxidation waves are observed at +0.54 and +0.79 V. When *tert*-butyl groups are introduced, there is a negative shift of the redox steps of 3b under the same conditions. It should be noted that when *n*-OC₁₆H₃₃ groups are connected to the *meso*-phenyl rings to form 3c, there are further shifts of the redox steps and a decrease in the gap between the 1st oxidation and reduction steps were observed in a similar manner to the narrowing in the predicted HOMO–LUMO gaps. The i_p^{Red} and i_p^{Ox} values, were determined from CV measurements for 3a-c made at various scan-rates from 20 to 500 mV (Fig. S7, see ESI), and this provides an insight into the reversibility of the system on an experimental time-scale. The good linear correlations observed for plots of peak current vs $v^{1/2}$ for 3a-c confirm that all of the oxidation and reduction processes are diffusion controlled.

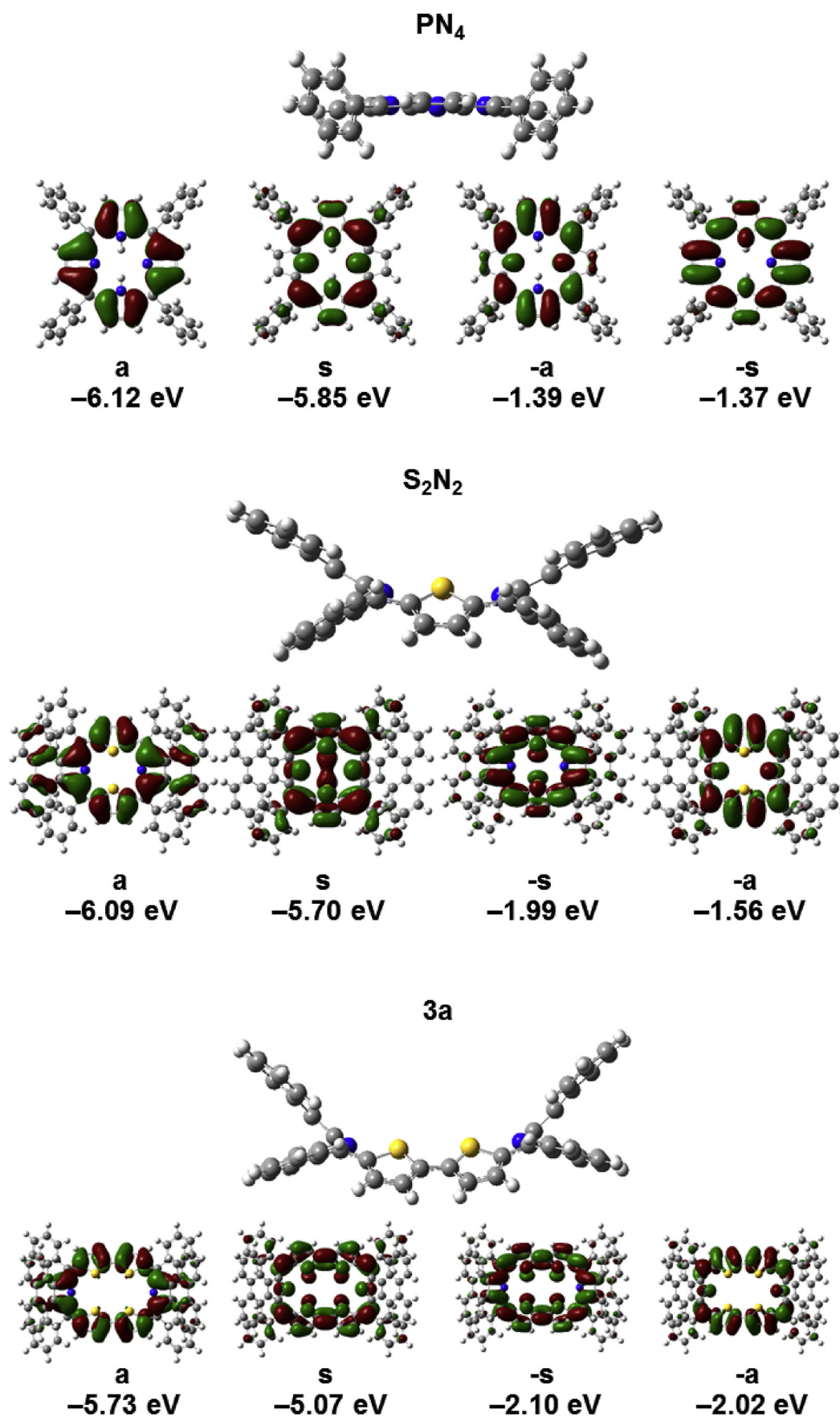


Fig. 1. The angular nodal patterns and the MO energies of the a, s, -a and -s MOs of the PN₄ and S₂N₂ model complexes and 3a at the CAM-B3LYP/6-31G(d) level of theory. The non-planarity of S₂N₂ and 3a are highlighted with views of the structures on the xz-plane.

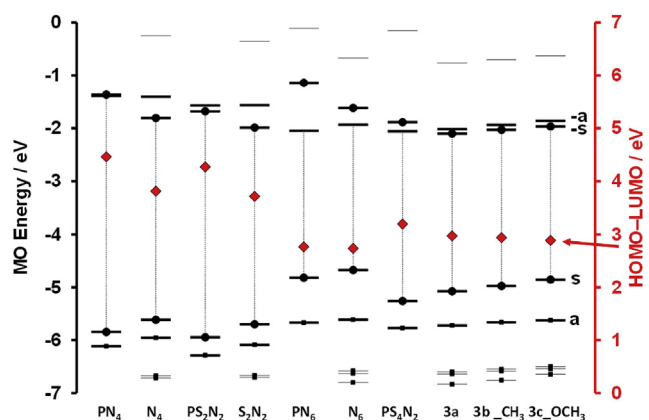


Fig. 2. Calculated MO energies of **3a-c** and a series of tetraphenylporphyrin (PN_4), tetraphenyldiphenanthroporphyrin (N_4), tetraphenyldithiaporphyrin (PN_2S_2), tetraphenyldiphenanthrodithiaporphyrin (N_2S_2), tetraphenylruberin (PN_6), tetraphenyldiphenanthroruberin (N_6), tetraphenyltetraathiaruberin (PS_4N_2) and tetraphenyldiphenanthrotetraathiaruberin (S_4N_2) model complexes at the CAM-B3LYP/6-31G(d) level of theory. Small black squares are used to highlight occupied MOs. The a, s, -a and -s are denoted with thicker black lines and black squares are used to highlight the s and -s MOs. Black circles are used to highlight the s and -s MOs. The HOMO-LUMO band gap values are highlighted with red diamonds and are plotted against a secondary axis. (For interpretation of the references to color in this figure legend, the reader is referred to the Web version of this article.)

3.4. Tunable and specific response with Hg^{2+} ions

Upon the addition of Ag^+ , Cu^{2+} , K^+ , Na^+ , Ca^{2+} , Ni^{2+} , Fe^{2+} , Fe^{3+} , Cd^{2+} , Cr^{2+} , Co^{3+} , Pb^{2+} and Pd^{2+} ion to water/DMF (v:v = 8:2) solutions of **3a-c**, no significant changes were observed in the UV-visible absorption spectra were observed in both the B and L band regions. In contrast, when Hg^{2+} was added to a similar solution of **3a** (Fig. 6), a significant decrease is observed in the intensity of the B band at ca. 590 nm probably due to interactions with the sulfur atoms that were introduced to the inner perimeter of the ruberin macrocycles. When a *p-tert*-butylphenyl substituent is introduced at the *meso*-positions of **3b**, a larger decrease in the B band intensity is observed. In contrast, in the case of **3c** which has a significantly longer lipophilic group on its *meso-p*- $\text{C}_{16}\text{H}_{33}\text{O}$ -phenyl rings, the main absorption band is shifted to longer wavelength to ca. 630 nm and the intensity decreases, but a clear B band remains apparent. When photographs of the water/DMF (v:v = 8:2) solutions of **3a-c** upon addition of 0.0–2.0 eq of Hg^{2+} are compared, the colorimetric changes that occur to generate (Fig. 7), purple (for **3a**), transparent (for **3b**) and blue (for **3c**) colors become apparent. The introduction of the lipophilic substituents of **3c** decreases the hydrophilic properties of the core-modified ruberins, and in the context of **3c** this could create a hydrophobic environment surrounding the inner cavity of the core-modified ruberin in highly polar and aqueous media. The selective response of the core-modified ruberin to Hg^{2+} ions can therefore be fine-tuned.

4. Conclusions

A series of core-modified and fused-ring-expanded ruberins have been synthesized and characterized, with the structures confirmed by MS and NMR data and elemental analyses. A series of spectroscopic, electrochemical measurements and TD-DFT calculations demonstrate that the modification of the inner perimeter of ruberins through core-modification with group 16 heteroatoms has a large influence on the electronic structure. In addition, these ruberins exhibit a highly selective and tuneable response to Hg^{2+} ions when lipophilic groups are introduced onto the *meso*-aryl rings. Considering NIR region dyes are being used in fields such as photo-energy conversion, dye-sensitized

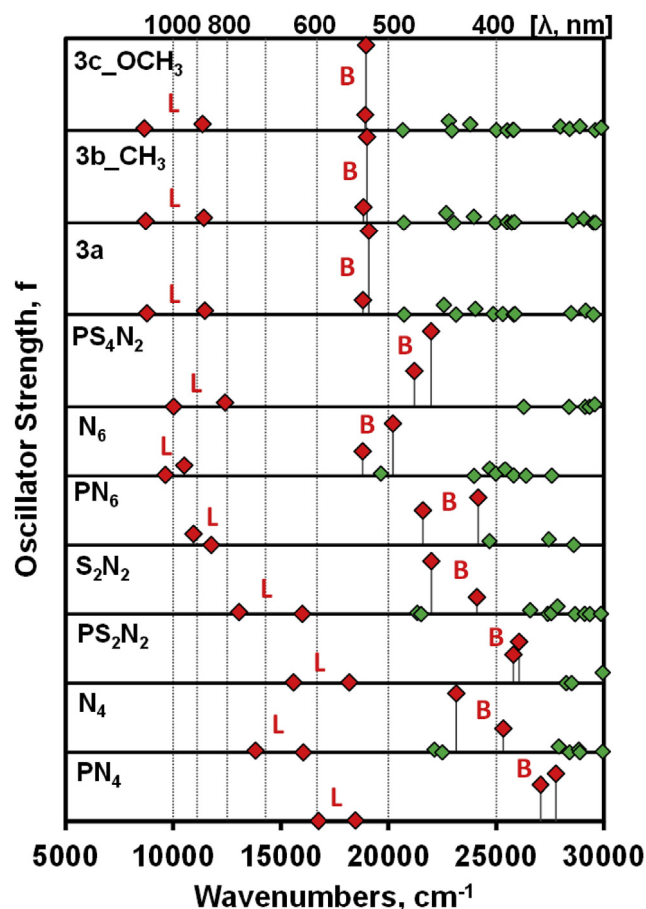


Fig. 3. Calculated TD-DFT spectra of **3a-c** and a series of tetraphenylporphyrin (PN_4), tetraphenyldiphenanthroporphyrin (N_4), tetraphenyldithiaporphyrin (PN_2S_2), tetraphenyldiphenanthrodithiaporphyrin (N_2S_2), tetraphenylruberin (PN_6), tetraphenyldiphenanthroruberin (N_6), tetraphenyltetraathiaruberin (PS_4N_2) and tetraphenyldiphenanthrotetraathiaruberin (S_4N_2) model complexes at the CAM-B3LYP/6-31G(d) level of theory. Red diamonds are used to highlight the L and B bands. Details of the calculations are provided in Table S1. (For interpretation of the references to color in this figure legend, the reader is referred to the Web version of this article.)

solar cells and toxic ion sensors, the modification of optical properties of ruberins revealed in this research is useful for the design of functional molecules based on conjugated systems of porphyrinoids.

Conflicts of interest

There are no conflicts of interests.

Acknowledgements

Financially supported by National Natural Scientific Foundation of China (No. 21701058 and 21301092), Natural Scientific Foundation of Jiangsu Province, P.R. China (No. BK20160499 and BK20151513), the fund from the State Key Laboratory of Coordination Chemistry (No. SKLCC1710, SKLCC1817), the fund from Key Laboratory of Functional Inorganic Material Chemistry (Heilongjiang University) of Ministry of Education, the Fok Ying Tung Education Foundation (Grant No. 141030) and Priority Academic Program Development of Jiangsu Higher Education Institutions (PAPD). The theoretical calculations were carried out at the Centre for High Performance Computing in Cape Town.

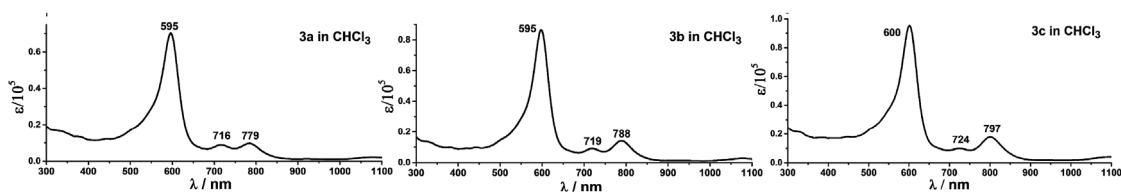


Fig. 4. UV-visible absorption spectra of rubryns **3a-c** in CHCl_3 .

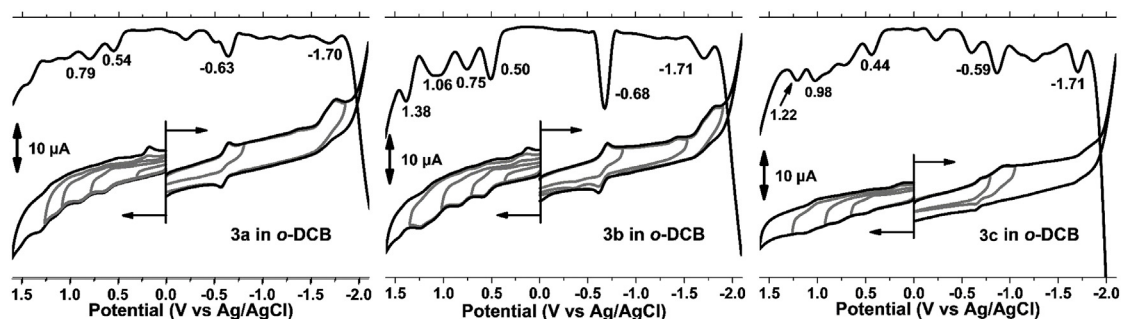


Fig. 5. CV and DPV measurements of rubryrin **3a-c** in *o*-dichlorobenzene (*o*-DCB) containing 0.1 M TBAP.

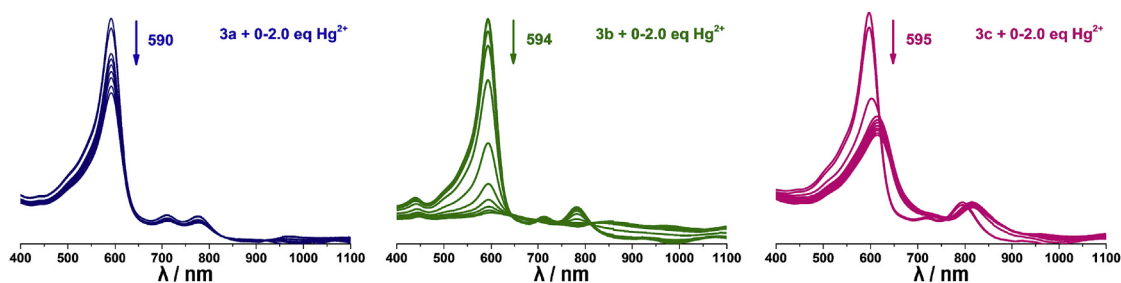


Fig. 6. UV-visible absorption spectra of **3a-c** (1.0×10^{-5} mol/L, in 80:20, DMF/water) upon addition of 0.0–2.0 eq of Hg^{2+} .

3a + 0.0–2.0 eq Hg^{2+}



3b + 0.0–2.0 eq Hg^{2+}



3c + 0.0–2.0 eq Hg^{2+}



Fig. 7. Photographs showing the colorimetric changes for **3a-c** in DMF/water ($v:v = 8:2$) solution upon addition of 0.0–2.0 eq of Hg^{2+} (left to right). The concentrations of **3a-c** are all closed to 1.0×10^{-5} mol/L.

Appendix A. Supplementary data

Supplementary data related to this article can be found at <http://dx.doi.org/10.1016/j.dyepig.2018.05.045>.

References

- [1] Shimizu S, Cho W, Sessler JL, Shinokubo H, Osuka A. *Chem Eur J* 2008;14:2668.
- [2] Kong J, Shao J, Li C, Qi D, Li M, Liang X, Zhu W, Jiang J, Xie Y. *Org Lett* 2017;19:650.
- [3] Li M, Wei P, Ishida M, Li X, Savage M, Guo R, Ou Z, Yang S, Furuta H, Xie Y. *Angew Chem Int Ed* 2016;55:3063.
- [4] Kumar R, Misra R, Chandrashekar TK, Nag A, Goswami D, Suresh E, Suresh CH. *Eur J Org Chem* 2007;27:4552.
- [5] Malakalappalli RRR, Mangalampalli R. *J Org Chem* 2011;76:3582.
- [6] Rao Y, Kim T, Park KH, Peng F, Liu L, Liu Y, Wen B, Liu S, Kirk SR, Wu L, Chen B, Ma M, Zhou M, Yin B, Zhang Y, Kim D, Song J. *Angew Chem Int Ed* 2016;55:6346.
- [7] Narayanan SJ, Sridevi B, Chandrashekar TK, Vij A, Roy R. *J Am Chem Soc* 1999;121:9053.
- [8] Liang X, Huang T, Li M, Mack J, Wildervanck M, Nyokong T, Zhu W. *Appl Catal A Chem* 2017;545:44.
- [9] Jiang Y, Li M, Liang X, Mack J, Wildervanck M, Nyokong T, Qin MF, Zhu WH. *Dalton Trans* 2015;44:18237.
- [10] Mack J. *Chem Rev* 2017;117:3444.
- [11] Geuenich D, Hess K, Kçhler F, Herges R. *Chem Rev* 2005;105:375.
- [12] Gouterman M. Dolphin D, editor. *The porphyrins. III Part A*. New York: Academic Press; 1978. p. 1–165.
- [13] Mack J, Kobayashi N. *Chem Rev* 2011;111:281.
- [14] Michl J. *J Am Chem Soc* 1978;100:6801.
- [15] Michl J. *J Am Chem Soc* 1978;100:6812.
- [16] Michl J. *Pure Appl Chem* 1980;52:1549.
- [17] Michl J. *Tetrahedron* 1984;40:3845.
- [18] Higashino T, Nakatsuji H, Fukuda R, Okamoto H, Imai H, Matsuda T, Tochio H, Shirakawa M, Tkachenko NV, Hashida M, Murakami T, Imahori H. *ChemBioChem* 2017;18:951.
- [19] Ahn TK, Kwon JH, Kim DY, Cho DW, Jeong DH, Kim SK, Suzuki M, Shimizu S,

- Osuka A, Kim D. *J Am Chem Soc* 2005;127:12856.
- [20] Yoon ZS, Kwon JH, Yoon MC, Koh MK, Noh SB, Sessler JL, Lee JT, Seidel D, Aguilar A, Shimizu S, Suzuki M, Osuka A, Kim D. *J Am Chem Soc* 2006;128:14128.
- [21] Rath H, Sankar J, Prabhuraja V, Chandrashekar TK, Nag A, Goswami D. *J Am Chem Soc* 2005;127:11608.
- [22] Parmeswaran D, Pushpan SK, Srinivasan A, Kumar MR, Chandrashekar TK, Ganesan S. *Photochem Photobiol* 2003;78:487.
- [23] Cappello T, Pereira P, Maisano M, Mauceri A, Pacheco M, Fasulo S. *Environ Pollut* 2016;219:139.
- [24] Valentino M, Santarelli L, Pieragostini E, Soleo L, Mocchegiani E. *Sci Total Environ* 2001;270:109.
- [25] Chen NY, Zhang YJ, Liu HY, Wu XX, Li YL, Miao LJ, Shen ZY, Wu AG. *ACS Sens* 2016;1:521.
- [26] Hossain KM, Kameyama T, Shibata T, Takagi K. *Bull Chem Soc Jpn* 2001;74:2415.
- [27] Pez D, Leal I, Gilberta IH. *Bioorg Med Chem* 2003;11:4693.
- [28] Novak BH, Lash TD. *J Org Chem* 1998;63:3998.